

bands correspond to even longer chains. Although the calculated frequencies correspond to the chains in the gas phase, the comparison with the helium data is still valid because the helium interactions are weak and the resulting frequency shifts small. The smooth dependence of the frequency shifts on cluster size, the agreement with *ab initio* calculations, the observed polarity of the complexes, and the assignment of their size on the basis of the pick-up cell pressure dependence of the corresponding signals combine to give overwhelming evidence that the clusters observed in this study were indeed linear chains.

The observation of these extended linear chains is quite surprising given that condensation occurs at very low temperatures. The condensation energy will be very rapidly quenched by the liquid helium, thus one might expect that the molecules would freeze on contact and be trapped in a range of local minima on the potential energy surface, resulting in many different isomers. The fact that we only observed linear chains implies that the molecules only make contact in a head-to-tail configuration. At the low temperatures of the helium droplets, the dipole-dipole interaction between an HCN monomer and an already formed chain is sufficient at a distance of 3 nm to effectively cause the two to orient in their mutual fields. In this strong-interaction regime, the dipole-dipole interaction is not motionally averaged to $1/R^6$. Therefore, when the molecules approach one another they are already oriented in such a way as to favor the formation of linear chains. When the molecules finally aggregate, the condensation energy is presumably dissipated so rapidly by the liquid helium that the system becomes trapped in the linear configuration, even though the dispersion interactions favor the cyclic structures. The situation is similar to the production of a glassy or amorphous phase by rapid quenching. Thus, the separation of the distance scales associated with the dipolar ($1/R^3$) and dispersion ($1/R^6$) interactions is crucial to this very selective self-assembly.

Although the *ab initio* calculations and the free jet expansion data agree that the linear HCN chains do not correspond to the global minima on the gas-phase potential energy surface, an important question to consider is if this is also true in liquid helium. Certainly, in analogy with the denaturing of proteins, if the interaction between the chains and the solvent is strong enough, the open chains, which optimize such interactions, will become favored. Although detailed theoretical calculations will be needed to include the effects of the helium solvent, a simple calculation based on the relative excluded volumes for linear and cyclic complexes indicates that the helium solvation energy is not sufficient to energetically favor the linear chains. Thus,

we conclude that the self-assembled chains observed here are fundamentally different from most self-assembled structures, in that they are not the minimum energy structures, nor are they in thermodynamic equilibrium.

One fundamental limit on the length of the chains that can be grown is the helium droplet diameter. A 10-molecule-long chain (~4 nm long) is about all that can fit within the present droplets once the evaporation of helium during the pick-up and condensation processes is taken into account. Another limitation for chain growth may have to do with the slow reorientation time associated with longer chains. As the moment of inertia of these long chains becomes very large, the reorientation needed to continue this self-assembly process may not be complete on the time scale for diffusion of the monomer unit. When this condition is reached, additional HCN monomers may attach to the sides of the chains, resulting in the formation of branched structures. Understanding these issues will be important for assessing the possibility and utility of extending this aggregation method to bulk liquid helium. Future studies should include examining the dependence of chain growth on the droplet size and attempting to grow long chains of water. In addition, more complex monomer units might be covalently linked after self-assembly, thus providing a new class of polar oligomers. Higher order moments (for example, quadrupole) could also potentially be used to self-assemble other structures.

References and Notes

1. J. O. Hirschfelder, C. F. Curtiss, R. B. Bird, *Molecular Theory of Gases and Liquids* (Wiley, New York, 1965).
2. J. N. Israelachvili, *Intermolecular and Surface Forces* (Academic Press, London, 1992).
3. W. J. Dulmage and W. N. Lipscomb, *Acta Crystallogr.* **4**, 330 (1951).
4. M. Kofranek, A. Karpfen, H. Lischka, *Chem. Phys.* **113**, 53 (1987).
5. I. J. Kurnig, H. Lischka, A. Karpfen, *J. Chem. Phys.* **92**, 2469 (1990).
6. A. Karpfen, *ibid.* **100**, 13474 (1996).
7. K. K. Lehmann and G. Scoles, *Science* **279**, 2065 (1998).
8. M. Hartmann, R. E. Miller, J. P. Toennies, A. F. Vilesov, *Phys. Rev. Lett.* **75**, 1566 (1995).
9. S. Goyal, D. L. Schutt, G. Scoles, *ibid.* **69**, 933 (1992).
10. M. Hartmann, R. E. Miller, J. P. Toennies, A. F. Vilesov, *Science* **272**, 1631 (1996).
11. S. Grebenev, J. P. Toennies, A. F. Vilesov, *ibid.* **279**, 2083 (1998).
12. L. W. Buxton, E. J. Campbell, W. H. Flygare, *Chem. Phys.* **56**, 399 (1981).
13. K. W. Jucks and R. E. Miller, *J. Chem. Phys.* **88**, 6059 (1988).
14. D. S. Anex, E. R. Davidson, C. Douketis, G. E. Ewing, *ibid.* **92**, 2913 (1988).
15. K. W. Jucks and R. E. Miller, *ibid.* **88**, 2196 (1988).
16. R. E. Miller, *Science* **240**, 447 (1988).
17. P. A. Block, E. J. Bohac, R. E. Miller, *Phys. Rev. Lett.* **68**, 1303 (1992).
18. P. A. Block, K. W. Jucks, L. G. Pedersen, R. E. Miller, *Chem. Phys.* **139**, 15 (1989).
19. C. M. Lovejoy and D. J. Nesbitt, *J. Chem. Phys.* **87**, 1450 (1987).
20. R. E. Miller, unpublished data.
21. T. E. Gough, M. Mengel, P. A. Rowntree, G. Scoles, *J. Chem. Phys.* **83**, 4958 (1985).
22. M. Lewerenz, B. Schilling, J. P. Toennies, *ibid.* **102**, 8191 (1995).
23. This work was supported by the NSF (CHE-97-10026). We also acknowledge the donors of The Petroleum Research Fund, administered by the American Chemical Society, for partial support of this research. We are grateful to E. Samulski and G. Scoles for several helpful discussions.

14 December 1998; accepted 8 February 1999

Epitaxial Cubic Gadolinium Oxide as a Dielectric for Gallium Arsenide Passivation

M. Hong,* J. Kwo, A. R. Kortan, J. P. Mannaerts, A. M. Sergent

Epitaxial growth of single-crystal gadolinium oxide dielectric thin films on gallium arsenide is reported. The gadolinium oxide film has a cubic structure isomorphous to manganese oxide and is (110)-oriented in single domain on the (100) gallium arsenide surface. The gadolinium oxide film has a dielectric constant of approximately 10, with low leakage current densities of about 10^{-9} to 10^{-10} amperes per square centimeter at zero bias. Typical breakdown field is 4 megavolts per centimeter for an oxide film 185 angstroms thick and 10 megavolts per centimeter for an oxide 45 angstroms thick. Both accumulation and inversion layers were observed in the gadolinium oxide-gallium arsenide metal oxide semiconductor diodes, using capacitance-voltage measurements. The ability to grow thin single-crystal oxide films on gallium arsenide with a low interfacial density of states has great potential impact on the electronic industry of compound semiconductors.

Effective passivation of III-V compound semiconductors (formed from elements of group III and V of the periodic table) finds

many applications in photonic and electronic devices. Intensive efforts have been made over the past 30 years in searching for elec-

REPORTS

trically and thermodynamically stable insulators on GaAs or other related III-V compound semiconductors (1-7). Specifically, an insulator of III-V compound semiconductor heterostructure showing a low interfacial state density (D_{it}) would provide a base for the long-sought metal oxide-semiconductor

field-effect transistors (MOSFETs) in III-V compound semiconductors.

Previously, we reported that in situ deposition of $Ga_2O_3(Gd_2O_3)$ dielectric film on GaAs surfaces by electron beam evaporation from single-crystal $Ga_3Gd_3O_{12}$ produced metal oxide-semiconductor (MOS) diode structures (6, 7) with a low D_{it} . Subsequent employment of $Ga_2O_3(Gd_2O_3)$ as a gate dielectric along with an ion implantation process led to the demonstration of the enhancement-mode GaAs MOSFETs

with inversion on semi-insulating GaAs substrates in both *n*- and *p*-channel configurations (8). We extended this oxide and the processing method to fabricate the insulated gate *n*-channel enhancement-mode InGaAs MOSFETs with inversion on InP semi-insulating substrates (9).

The fundamental cause responsible for such a remarkably low interfacial state density near the $Ga_2O_3(Gd_2O_3)/GaAs$ interface is not clear. Low D_{it} values were not obtained in other oxide/GaAs systems, such as MgO , SiO_2 , and Al_2O_3 prepared by a similar approach (6, 10). Furthermore, in a separate experiment employing pure Ga_2O_3 films that were in situ electron-beam-evaporated from a Ga_2O_3 powder-packed source, the GaAs surfaces were not effectively passivated (11). These results suggest the necessity of Gd_2O_3 .

We report successful growth of a new dielectric oxide, Gd_2O_3 , as a film to passivate GaAs surface. Contrary to expectations that the $Ga_2O_3(Gd_2O_3)$ films would be amorphous, we found that the electron beam-evaporated Gd_2O_3 film is a single crystal epitaxially grown in (110) orientation on the GaAs (100) surface. Structural studies indicate the epitaxy takes place in single-domain growth over an oxide thickness from 25 to at least 400 Å. The electrical measurements show that Gd_2O_3 is an excellent dielectric, with a dielectric constant (ϵ) of ~ 10 . Furthermore, both inversion and accumulation layers were observed in the $Gd_2O_3/GaAs$ MOS diodes.

Growth of $Gd_2O_3/GaAs$ heterostructures was performed in a multichamber ultrahigh vacuum system under conditions similar to our previous work (6, 12) on $Ga_2O_3(Gd_2O_3)$. A powder-packed Gd_2O_3 source was used for electron beam evaporation. The substrate temperature was held at $\sim 200^\circ$ to $550^\circ C$. During deposition, in situ reflection high-energy electron diffraction (RHEED) was used to monitor the growth process. Oxide film thickness was determined by ellipsometry and x-ray reflectivity (13). The structural properties were characterized by x-ray diffraction using a rotating anode source equipped with a triple-crystal four-circle diffractometer (14). The current-voltage (I-V) and capacitance-voltage (C-V) measurements were taken by standard methods. We evaporated Au/Pt dots of 75, 100, and 150 μm in diameter to the oxide surface to serve as electrical contacts. The other probe was placed to the back of the GaAs substrate for both the I-V and C-V measurements.

The in situ RHEED patterns (Fig. 1) illustrate the growth sequence of the single-crystal Gd_2O_3 film surface. Before oxide deposition, an arsenic-stabilized (100) GaAs surface was obtained after heating the substrate to $550^\circ C$ (Fig. 1A). A Gd_2O_3

Bell Laboratories, Lucent Technologies, Murray Hill, NJ 07974, USA.

*To whom correspondence should be addressed. E-mail: mwh@lucent.com

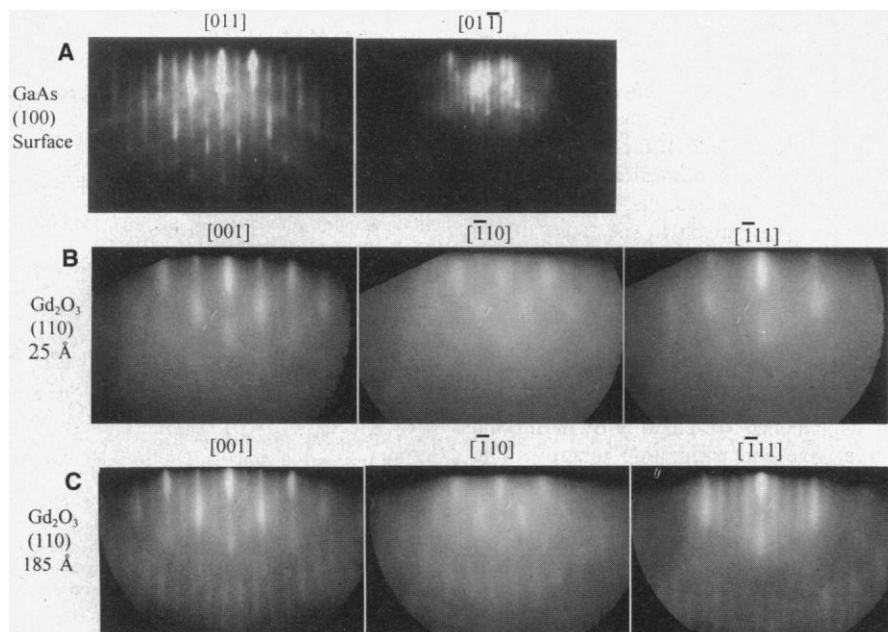


Fig. 1. In situ RHEED patterns of (A) (100) GaAs surface along the [011] and [01 $\bar{1}$] axes; (B) (110) Gd_2O_3 film 25 Å thick along the [001], [$\bar{1}10$], and [$\bar{1}\bar{1}1$] axes; and (C) (110) Gd_2O_3 film 185 Å thick along same axes.

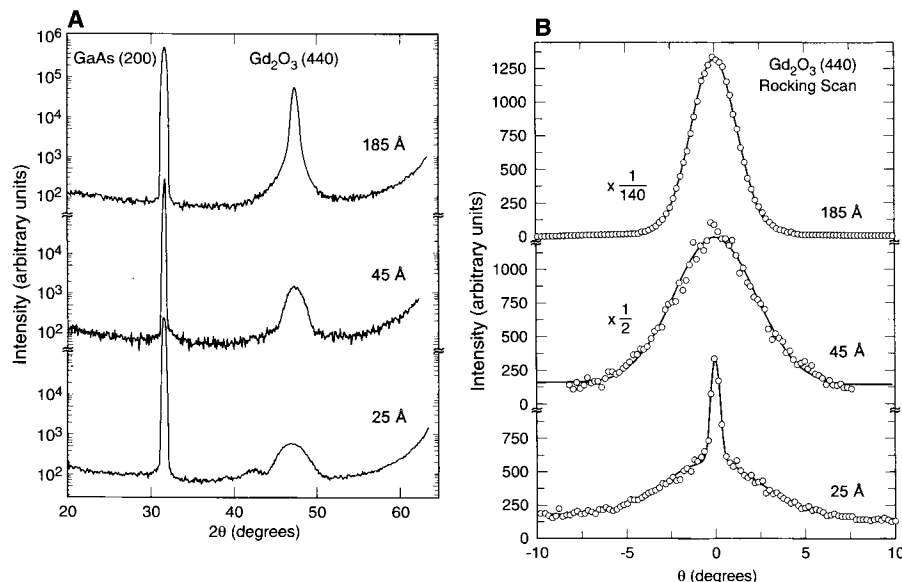


Fig. 2. (A) X-ray θ - 2θ scans of the (440) Bragg reflection of the (110)-oriented Gd_2O_3 films of 185, 45, and 25 Å thickness. (B) Rocking curve scans of these peaks about the θ angle for the three samples in (A).

film 25 Å thick results in streaky RHEED patterns of twofold symmetry (Fig. 1B). Analysis of the diffraction patterns indicates that the Gd₂O₃ film is (110)-oriented and grown in single domain. The in-plane epitaxial relationship between (100) GaAs substrate and (110) Gd₂O₃ film is [001]_{Gd₂O₃} // [011]_{GaAs} and [110]_{Gd₂O₃} // [011]_{GaAs}. Judging from the sharper streak patterns in Fig. 1C, the epitaxial growth continues and is not limited to a thickness of 185 Å.

X-ray diffraction measurements were performed along surface normal (110) Gd₂O₃ films of 185, 45, and 25 Å thickness (Fig. 2A). The 185 Å sample revealed a diffraction peak at the bulk (440) peak position along the colinear direction with the GaAs (200) peak. Additional single-crystal scans made on this sample confirmed the bulk structure as isomorphic to Mn₂O₃ archived in powder diffraction file data bank (15). The 45 Å-thick film did not show a substantial shift in the surface normal direction, indicating that the films are mostly relaxed with no strain built up. This is confirmed with the rocking scans (Fig. 2B), which show substantial broadening over the instrument resolution of 0.25°, indicating that films have a mosaic spread, possibly caused by dislocations. The 25 Å-thick film, however, shows a very sharp component in the rocking scan, meaning that the epitaxial film, at such a fine thickness, elastically distorts its unit cell in order to conform to the in-plane perfect epitaxial condition. As the film grows thicker, it becomes energetically more favorable to relax the strain by generating misfit dislocations.

Additional x-ray scans to confirm that Gd₂O₃ film is indeed of single domain were done by fixing the detector to the lattice spacing of the (222) reflection of the oxide, and then rotating the sample (ω angle) 360° on a cone centered to the surface normal. Observed reflections unequivocally suggest a nearly perfect epitaxial growth of a single-domain, single-crystal Gd₂O₃ film on GaAs (100). This is unusual considering the twofold degeneracy of aligning the (110) Gd₂O₃ plane of a rectangular symmetry onto the square symmetric (100) GaAs surface. The attainment of single domain is attributed to the (2×4) reconstruction occurring on the GaAs surface that removes the twofold degeneracy, thus favoring the single variant growth. We also found that Gd₂O₃ film grows in single domain on a Ga-stabilized (4×6) reconstructed GaAs surface.

Gadolinium oxide is an ionic crystal with a large lattice constant of 10.81 Å. In contrast, GaAs bonds covalently and has a lattice constant of 5.65 Å. The in-plane

epitaxy of [001] Gd₂O₃ that is parallel with [011] GaAs suggests a super-cell lattice match—that is, the spacing of three Gd₂O₃ [001] lattices (32.4 Å) matches that of four GaAs [011] lattices (32 Å). This epitaxy occurring at the interface of two vastly dissimilar systems is quite complex. The first report of epitaxial oxide/GaAs heterostructure was MgO on GaAs (100) (16).

The Gd₂O₃ dielectric films are highly electrically insulating, showing very low leakage current densities of $\sim 10^{-9}$ to 10^{-10} A/cm² at zero bias. This may have to do with that fact that Gd is electropositive +3 and has a strong affinity to oxygen. We measured the dependence of the leakage current density (J_L) on the applied field (E) for a set of Gd₂O₃ samples with the oxide thickness (t_{ox}) systematically reduced from 260 to 25 Å (Fig. 3). The positive bias means that the metal electrode is positive with respect to GaAs. As t_{ox} is decreased from 260 to 45 Å, the respective breakdown field E_{br} increases systematically from 3 to 10 MV/cm, yet J_L in-

creases merely by one order of magnitude. The maintenance of low electrical leakage even for films as thin as 25 Å suggests that a high degree of structural integrity is sustained through epitaxy.

Depositions at temperatures >600°C produced films of poor electrical properties due to chemical reaction with the GaAs substrates. However, once the single-crystal Gd₂O₃ films are formed at optimum growth temperatures below 600°C, they are thermodynamically stable. When subjected to 850°C annealing for postgrowth processing, the C-V measurements still show the accumulation and inversion, and there is little change in the I-V curves, indicating that the Gd₂O₃-GaAs interfaces remained intact under such severe temperature stress. Moreover, we have successfully fabricated a GaAs MOSFET using the Gd₂O₃-GaAs samples, demonstrating that the Gd₂O₃-GaAs interfaces survived under severe processing conditions (17). These results suggest that the presence of surface stress in the heterostructure does not impede device

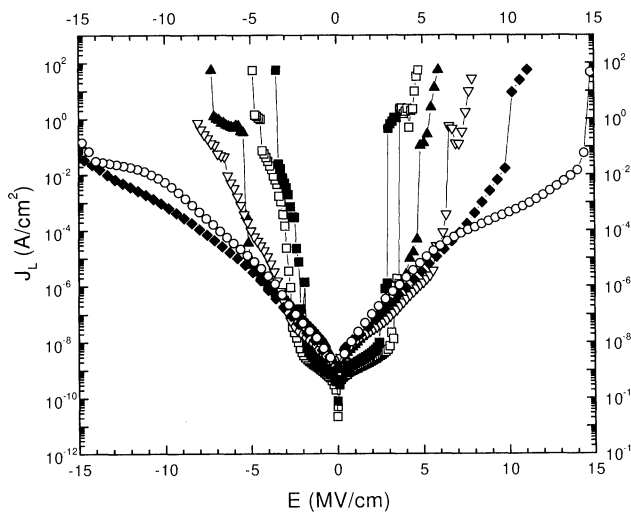


Fig. 3. Leakage current density J_L versus electrical field E for Gd₂O₃ films with decreasing thickness of 260 (■), 185 (□), 140 (▲), 104 (▽), 45 (◆), and 25 Å (○).

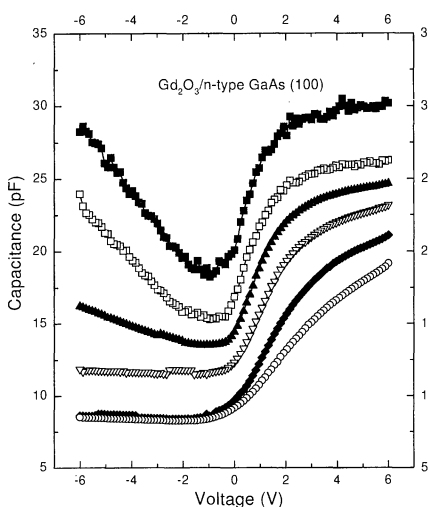


Fig. 4. C-V traces for a MOS diode made of a Gd₂O₃ film 185 Å thick on GaAs with an n-type doping of 4×10^{17} cm⁻³ under various frequencies of 50 Hz (■), 100 Hz (□), 1 kHz (▼), 10 kHz (▽), 100 kHz (◆), and 1 MHz (○). The measured area is 4.4×10^{-5} cm².

fabrication. Nevertheless, the effects of the surface stress on the oxide and consequently on the lifetime and the reliability of the devices are important issues and need to be addressed further.

In the C-V traces of a MOS diode made of the Gd_2O_3 of 185 Å thickness (Fig. 4), a transition from accumulation to depletion mode occurs at ~ 2 V. The inversion carriers (holes) follow the ac signal up to a frequency of 10 kHz and do not respond to frequencies greater than 100 kHz. This compares favorably to previous samples of $Ga_2O_3(Gd_2O_3)$ films on GaAs, in which the inversion carriers followed the ac signal only up to a frequency of 1 kHz (7). There is some hysteresis in the C-V curves in reverse sweeping, with the widest spread of no more than 1 V. These curves remain the same after repeated voltage cycles.

The C-V characteristics can be further understood by taking the conductance (G) into account. The finite value of G is in parallel with the oxide capacitance (C_{ox}). This simple equivalent circuit model explains that the total capacitance increases as the modulation frequency decreases. After replotting the C-V curves by subtracting the contributions from G and C_{ox} , the D_{it} , which responds only to the low-frequency measurements, can be deduced from the high- and low-frequency curves. D_{it} at the midgap is $\sim 10^{11} \text{ cm}^{-2} \text{ eV}^{-1}$, which is slightly higher than those of the SiO_2/Si interfaces.

We expect that epitaxial growth of structures isomorphous to that of Mn_2O_3 can be extended to other rare earth oxides and to other semiconductor substrates like Si. Our findings thus suggest new opportunities for producing high- ϵ gate dielectrics for Si- and GaAs-based MOSFETs.

References and Notes

1. A. Revesz and K. Zaininger, *J. Am. Ceram. Soc.* **46**, 606 (1963).
2. O. Weinreich, *J. Appl. Phys.* **37**, 2924 (1966).
3. T. Mimura, K. Odani, N. Yokoyama, Y. Nakayama, M. Fukuta, *IEEE Trans. Electron Devices* **25**, 573 (1978).
4. W. T. Tsang, *Appl. Phys. Lett.* **33**, 429 (1978).
5. C. W. Wilmsen, Ed., *Physics and Chemistry of III-V Compound Semiconductor Interfaces* (Plenum, New York, 1985).
6. M. Hong et al., *J. Vac. Sci. Technol. B* **14**, 2297 (1996).
7. M. Passlack et al., *IEEE Trans. Electron Devices* **44**, 214 (1997).
8. F. Ren et al., *Technical Digest of the IEEE, International Electron Devices Meeting*, San Francisco, CA, 8 to 11 December 1996 (IEEE, Piscataway, NJ, 1996), pp. 943–945.
9. F. Ren et al., *IEEE Electron Device Lett.* **19**, 309 (1998).
10. L. W. Tu, E. F. Schubert, M. Hong, G. J. Zydzik, *J. Appl. Phys.* **80**, 6448 (1996).
11. J. Kwo et al., *J. Vac. Sci. Technol. B*, in press.
12. M. Hong, *J. Cryst. Growth* **150**, 277 (1995).
13. M. Hong et al., *J. Vac. Sci. Technol. B* **16**, 1395 (1998).
14. A. R. Kortan, A. Erbil, R. J. Birgeneau, M. S. Dresselhaus, *Phys. Rev. Lett.* **47**, 1206 (1981).
15. S. Geller, *Acta Crystallogr. B* **27**, 821 (1971).

16. K. Nashimoto, D. K. Fork, T. H. Geballe, *Appl. Phys. Lett.* **60**, 1199 (1992).
17. Y. C. Wang, M. Hong, J. Kwo, J. P. Mannaerts, unpublished results.
18. We would like to thank A. Y. Cho, R. M. Fleming,

T. S. Lay, C. T. Liu, D. W. Murphy, G. L. Timp, R. B. van Dover, Y. H. Wong, and M. C. Wu for valuable suggestions.

19 October 1998; accepted 8 February 1999

Degradation Mechanism of Small Molecule-Based Organic Light-Emitting Devices

Hany Aziz,¹ Zoran D. Popovic,^{2*}
Nan-Xing Hu,² Ah-Mee Hor,² Gu Xu¹

Studies on the long-term degradation of organic light-emitting devices (OLEDs) based on tris(8-hydroxyquinoline) aluminum (AlQ_3), the most widely used electroluminescent molecule, reveal that injection of holes in AlQ_3 is the main cause of device degradation. The transport of holes into AlQ_3 caused a decrease in its fluorescence quantum efficiency, thus showing that cationic AlQ_3 species are unstable and that their degradation products are fluorescence quenchers. These findings explain the success of different approaches to stabilizing OLEDs, such as doping of the hole transport layer, introducing a buffer layer at the hole-injecting contact, and using mixed emitting layers of hole and electron transporting molecules.

Because of their high brightness (1, 2) and the availability of a wide range of emission colors (3, 4), OLEDs have the potential to achieve low-cost, full-color flat-panel displays. However, OLEDs show relatively poor stability. The half-lifetime, defined as the time elapsed before the luminance of the OLED decreases to half its initial value, usually amounts to only few hundred hours (4). In general, degradation in OLEDs occurs through the formation of nonemissive “dark” spots as well as through a long-term “intrinsic” decrease in the electroluminescence (EL) efficiency of the devices during operation (5). Although the mechanisms that cause dark spots have been identified (5, 6) and controlled (7), the causes of intrinsic degradation remain unclear. In the devices based on small organic molecules, introduction of dopants in the hole transport layer (HTL) (8) or a buffer layer at the hole-injecting contact (9) was found to significantly reduce the intrinsic degradation. Half-lifetimes exceeding 4000 hours, at an initial luminance of 500 cd/m^2 , have been achieved for devices with a copper phthalocyanine (CuPc) buffer layer (9). The life and efficiency of these devices is further extended by doping the AlQ_3 with N,N -dimethylquinacridone (10). Morphological changes in the HTL or degradation at the hole-injecting contact were specul-

ed to cause degradation in the OLEDs, but the occurrence of such processes in OLEDs or their role in degradation has never been verified. In fact, other reports show no correlation between the morphological stability of the HTL and the lifetime of the OLEDs (11).

We investigated OLEDs based on AlQ_3 , the most widely used electroluminescent molecule, and found that injection of holes in AlQ_3 was the main factor responsible for device degradation. Photoluminescence (PL) quantum efficiency of AlQ_3 layers, where predominantly holes are transported, decreased upon prolonged current flow (12). These findings naturally explain different approaches to stabilizing OLEDs, such as doping of the HTL (8), introducing a CuPc buffer layer at the hole-injecting contact (9), or using a mixed emitting layer of hole and electron transporting molecules (13).

We previously found that using a mixed emitting layer of hole and electron transporting molecules, placed between pure hole and electron transport layers (ETLs), dramatically increased LED stability (13). These devices show a half-lifetime of about 1400 hours at an initial luminance of about 1000 cd/m^2 (versus tens of hours for devices with pure layers), despite not having a doped HTL or a buffer layer at the hole-injecting contact (Fig. 1). This result suggests that device aging at room temperature is not caused by morphological changes in the HTL or degradation at the indium-tin-oxide (ITO)-HTL interface. This is not necessarily the case for hole transport molecules with low glass transition tempera-

¹Department of Materials Science and Engineering, McMaster University, Hamilton, Ontario, Canada.

²Xerox Research Centre of Canada, Mississauga, Ontario, Canada.

*To whom correspondence should be addressed.